

# Quantum learning advantage on a scalable photonic platform

Zheng-Hao Liu<sup>¶,1,\*</sup> Romain Brunel<sup>1,\*</sup> Emil E. B. Østergaard<sup>1</sup> Oscar Cordero<sup>1</sup> Senrui Chen,<sup>2</sup>  
Yat Wong,<sup>2</sup> Jens A. H. Nielsen,<sup>1</sup> Axel B. Bregnsbo,<sup>1</sup> Sisi Zhou,<sup>3,4</sup> Hsin-Yuan Huang,<sup>5,6,7</sup>  
Changhun Oh,<sup>8</sup> Liang Jiang,<sup>2</sup> John Preskill,<sup>6</sup> Jonas S. Neergaard-Nielsen,<sup>1</sup> and Ulrik L. Andersen<sup>1,†</sup>

<sup>1</sup>*Center for Macroscopic Quantum States (bigQ), Department of Physics,  
Technical University of Denmark, Fysikvej, 2800 Kongens Lyngby, Denmark*

<sup>2</sup>*Pritzker School of Molecular Engineering, The University of Chicago, Chicago, Illinois 60637, USA*

<sup>3</sup>*Perimeter Institute for Theoretical Physics, Waterloo, Ontario N2L 2Y5, Canada*

<sup>4</sup>*Department of Physics and Astronomy and Institute for Quantum Computing,  
University of Waterloo, Ontario N2L 2Y5, Canada*

<sup>5</sup>*Google Quantum AI, Venice, CA, USA*

<sup>6</sup>*Institute for Quantum Information and Matter,*

*California Institute of Technology, Pasadena, CA 91125, USA*

<sup>7</sup>*Center for Theoretical Physics, Massachusetts Institute of Technology, Cambridge, MA 02139, USA*

<sup>8</sup>*Department of Physics, Korea Advanced Institute of Science and Technology, Daejeon 34141, Korea*

(Dated: February 12, 2025)

Recent advancements in quantum technologies have opened new horizons for exploring the physical world in ways once deemed impossible. Central to these breakthroughs is the concept of quantum advantage, where quantum systems outperform their classical counterparts in solving specific tasks. While much attention has been devoted to computational speedups, quantum advantage in learning physical systems remains a largely untapped frontier. Here, we present a photonic implementation of a quantum-enhanced protocol for learning the probability distribution of a multimode bosonic displacement process. By harnessing the unique properties of continuous-variable quantum entanglement, we obtain a massive advantage in sample complexity with respect to conventional methods without entangled resources. With approximately 5 dB of two-mode squeezing—corresponding to imperfect Einstein–Podolsky–Rosen (EPR) entanglement—we learn a 100-mode bosonic displacement process using 11.8 orders of magnitude fewer samples than a conventional scheme. Our results demonstrate that even with non-ideal, noisy entanglement, a significant quantum advantage can be realized in continuous-variable quantum systems. This marks an important step towards practical quantum-enhanced learning protocols with implications for quantum metrology, certification, and machine learning.

Learning the properties of a physical system by performing measurements on it is at the foundation of natural sciences. In conventional settings, this typically involves collecting a large set of independent measurements of certain variables of the system and applying statistical methods on a classical computer to estimate their underlying distribution, from which the properties of the system can be inferred. However, in quantum systems, the learning task is hindered by the constraints of quantum physics, such as the inherent quantum noise associated with measurements, encapsulated by Heisenberg’s uncertainty principle. Consequently, the sample complexity—the number of experiments required to learn certain properties of quantum systems—can scale exponentially with the system size, rendering some learning tasks practically infeasible using classical, conventional learning approaches [1, 2].

As an alternative to the conventional approach of using independent probe states and a classical processor for data analysis, quantum learning strategies have been proposed [3–10]. In such approaches, the probe states are not measured independently but instead undergo a collective quantum algorithmic measurement before data analysis is conducted. By leveraging quan-

tum coherence of the probe states and collective measurements, it has been shown that, for certain finite-dimensional quantum systems, the sample complexity required to learn some of their underlying properties can be dramatically reduced, with an exponentially smaller number of experiments required to complete the task [3, 9]. Building on these ideas, quantum advantage in learning was first demonstrated on a superconducting electronic platform [11]. By utilizing 20 qubits as a probe state, a learning task was accomplished using approximately  $10^5$  fewer samples than conventional methods. Given the system size limit for superconducting systems and the challenges in capturing and transducing unknown quantum states into superconducting qubits, it is particularly intriguing to address how a scalable quantum learning advantage can be achieved in more practical scenarios.

In our work, we significantly advance the frontier of quantum learning by demonstrating an unprecedented quantum advantage, achieving orders-of-magnitude improvement on a scalable continuous-variable (CV) photonic platform. Using an ensemble of imperfect EPR entangled states of light and a joint CV measurement approach, we successfully learn the amplitude and phase distributions of a multi-mode displacement process with  $10^{11}$  times fewer samples than required by an approach without entanglement. Furthermore, our photonic platform enables a significant quantum advantage in distinguishing two families

¶ zheli@dtu.dk

\* These authors contributed equally to this work.

† ulrik.andersen@fysik.dtu.dk

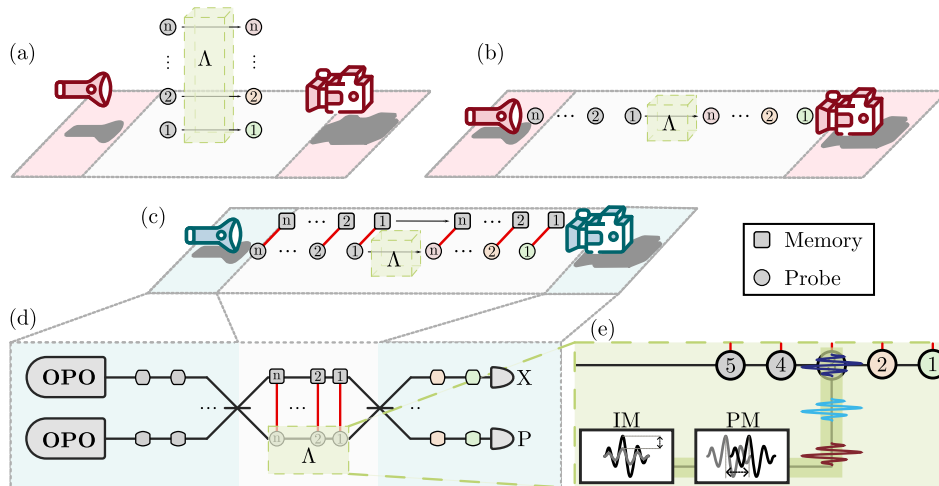


Fig. 1. **Quantum entanglement-enhanced learning with photons.** (a) Conventional learning of a channel. A multi-mode probe state is sent through a channel, followed by a measurement of the probe state to extract the information about the channel. (b) Conventional learning of a multi-time physical process, where the measurement settings are allowed to be adaptive within a sample. We show that for both (a) and (b), a fundamental entanglement-free complexity bound applies to the required sample overhead for the learning task. (c) Quantum entanglement-enhanced learning of a multi-time process. The probe state is allowed to be entangled with an external memory state. The joint measurement of both states makes overcoming the classical complexity limit possible. (d) Implementation of quantum learning with squeezed light. Two-mode squeezing is generated by interfering the outputs of two optical parametric oscillators (OPOs). One of the spatial modes is temporally-multiplexed and used as the probe state while the other is used as the memory. The physical process to be learned is a phase-space random displacement. A Bell measurement between the corresponding modes of the probe and memory states works to extract the information. (e) We realize the displacement process by mixing a frequency-shifted coherent state into the probe. The frequency-shifted coherent state is shaped by two electro-optic modulators, an intensity modulator (IM) and a phase modulator (PM).

of quantum processes. Our implementation, capable of learning an infinite-dimensional joint displacement process spanning over 100 modes, tackles problems whose complexity substantially surpasses the previous superconducting qubit-based demonstration [11]. The photonic CV platform [12], a natural architecture for quantum information processing, has been at the forefront in advancing quantum technologies—from boson sampling [13, 14] to quantum communication [15–17], computation [18–20], and sensing [21–23]. This work demonstrates how photonic systems, with their established capabilities in computation and sensing, can be leveraged to enhance our ability to learn about physical systems. Moreover, while photonic systems have previously demonstrated their potential in various areas of quantum information processing, a definitive quantum advantage in such systems has not been achieved until now [24]. Our achievement thus represents an important milestone in both quantum learning and the broader field of quantum information science.

*Context.*—The task of quantum learning proceeds as follows: The experimenter aims to learn a specific property of a quantum system, such as the probability distribution of a quantum state or the noise characteristics of a particular quantum device. The experimenter probes the device  $N$  times, yielding  $N$  data samples (See Fig. 1(a)), from which the target property or probability distribution is reconstructed with a certain precision or classified with a specified confidence.

In this work, we focus on the task of learning the properties of random  $n$ -mode phase-space displace-

ment processes, which model the physical process of random amplitude and phase noise in bosonic channels. These channels are of particular interest because any CV noise channel can be tailored into a random displacement channel by twirling with displacement operators, similar to Pauli twirling in DV systems [25]. Moreover, learning the properties of multi-time displacement processes has broad applications including gravitational wave detection [26, 27], Raman spectroscopy [28, 29], dark matter searches [30, 31], and microscopic force sensing [32].

We learn the dynamical displacement process, labeled  $\Lambda$ , by probing it with quantum states of light, followed by measurements that extract information about the probability distribution  $p(\alpha)$  of the  $n$ -mode displacement process, where  $\alpha$  is the  $n$ -dimensional complex-valued vector describing the phase-space displacement. We refer the readers to the Supplementary Material Sec. IIA for the formal definition of the displacement process. The key challenge is to resolve sub-Planck features of phase space with the highest possible resolution. This is accomplished through a sequence of  $N$  samples using carefully chosen probe states and measurement schemes to reconstruct  $p(\alpha)$  or test properties of the displacement process.

The fundamental challenge in this learning task can be understood through the characteristic function  $\lambda(\beta)$ , which is defined over the dual space of the  $n$ -mode displacement channel. Mathematically,  $\lambda(\beta)$  is the Fourier transform of the phase-space probability distribution  $p(\alpha)$ . The high-frequency components of  $\lambda(\beta)$ , i.e., regions where  $|\beta|^2$  is large, encode the fine

structure of the displacement channel. In a previous work by some of us [8], we proved that learning  $\lambda(\beta)$  to a fixed accuracy within a hyperball of squared radius  $|\beta|^2 \propto n$  requires a number of samples scaling exponentially in the number of modes  $n$ . Here, we extend this result to prove (cf. Supplementary Material, Theorem 3) that the same lower bound for sample complexity, hereafter referred to as the classical complexity bound, still applies even when the channel is implemented as a multi-time process (as depicted in Fig. 1(b)), and an adaptive strategy is allowed for the measurement. Notably, this exponential scaling in sample complexity is fundamental—it holds for any choice of probe state that is not entangled with an external quantum memory.

*Quantum-enhanced learning.*—We use entanglement to overcome this limitation on learning a random displacement process. Our quantum-enhanced learning scheme, illustrated in Fig. 1(c), fundamentally differs from conventional entanglement-free approaches: each probe mode in the probing state is entangled with a corresponding auxiliary memory mode, forming EPR entangled (or two-mode squeezed) states of a certain squeezing level. The learning process is carried out by sending the probe modes through the displacement process, and subsequently performing pairwise CV Bell measurements on the probe and memory modes. These Bell measurements are joint measurements that simultaneously reveal the quantum correlations between the two modes’ amplitude and phase quadratures, thereby bypassing the limitation imposed by the uncertainty principle for individual measurements. In Supplementary Material Sec. IIB, we describe the method for estimating the characteristic function from the measured samples. It allows for efficient extraction of information about the displacement process with a phase-space resolution given by the amount of entanglement. For instance, in the ideal case where the probe and memory modes form perfect EPR states (corresponding to infinite squeezing), the quadratures of the probe and memory modes before the random displacement are perfectly correlated. Any observed deviation from these perfect correlations during the Bell measurement can be attributed solely to the effect of the displacement process. In this scenario, the protocol can extract the complete information of the process without introducing additional noise, demonstrating its potential for noise-free learning.

We realize the quantum-enhanced learning protocol in a CV optical setup, as illustrated in Fig. 1(d), with a detailed description provided in Supplementary Material Sec. I. The two-mode squeezed vacuum states, comprising the probe and memory modes, are generated by interfering the outputs of two optical parametric oscillators (OPOs). Each mode is defined in the temporal domain of the squeezed light, represented by its electromagnetic field weighted by a mode function—a Gaussian-modulated (full-width half-max of 320 ns) 3.8 MHz sine wave. Multiple modes are created consecutively at the continuously generated OPO outputs, enabling us to scale up the number of modes for the learning task and achieve a substantial quan-

tum advantage. The displacement process is implemented by mixing a weak coherent state into the probe modes via an unbalanced beam splitter (cf. Fig. 1(e)). By matching the coherent state’s temporal mode function and varying its complex amplitude using a pair of electro-optic modulators, we induce a multi-mode correlated displacement. To extract the displacement information, we perform Bell measurements by interfering the probe and memory modes and using homodyne detection to measure the amplitude and phase quadratures of the resulting output signals. Our OPOs achieve up to 68% reduction of noise power during Bell measurements, enabling high precision in detecting the effects of the process.

*Process reconstruction.*—We demonstrate the quantum enhancement of the learning task by reconstructing the characteristic function  $\lambda(\beta)$  of a class of three-peak displacement processes, defined in Supplementary Material, Definition S4, using Bell measurement outcomes. We denote the reconstructed characteristic function as  $\tilde{\lambda}(\beta)$ . For a fixed squeezing parameter  $r$ , achieving a given reconstruction accuracy requires  $N \sim \exp(2e^{-2r}|\beta|^2)$  samples, which grows exponentially with  $|\beta|^2$ . When the number of samples  $N$  is insufficient, the reconstructed characteristic function  $\tilde{\lambda}(\beta)$  can diverge at large  $|\beta|^2$ . To visualize this divergence behavior, we plot the reconstructed characteristic function along a slice  $\beta_0 = b(1, 1, \dots, 1)$ ,  $b \in [0, 0.5]$  in the high-dimensional dual space in Fig. 2(a): without squeezing ( $r = 0$ ), the reconstructed 16-mode characteristic function from 200 samples diverges rapidly and fails to capture the ground truth’s peak at  $b = 0.3$ . Furthermore, extending the radius  $|\beta|$  of the reconstructable hyperball requires a substantial increase in sample complexity: approximately  $10^5$  samples are needed to reveal the peak at  $b = 0.3$ .

The introduction of moderate entanglement through two-mode squeezing ( $r > 0$ ) dramatically reduces this sample complexity. As shown in Fig. 2(b), when the number of modes increases to 30, reconstruction without entanglement ( $r = 0$ ) fails even with  $10^5$  samples, requiring an impractically large number of samples. However, with moderate entanglement, faithful reconstruction becomes achievable with the same number of samples. To systematically investigate the effect of entanglement on sample complexity across different numbers of modes, we measure the two-mode squeezed vacuum state under various  $n$ -mode displacement processes using three distinct two-mode squeezing levels: 0 dB,  $-2.26$  dB, and  $-4.78$  dB. Notably, during the 4.78 dB realization, the squeezing increased to 4.95 dB for mode numbers 60 and 80. We characterize the reconstruction performance using  $(\epsilon, \delta)$ -complexity: the number of samples required to reconstruct  $\lambda(\beta)$  with precision  $\epsilon$ , such that  $|\lambda(\beta) - \tilde{\lambda}(\beta)| < \epsilon$  for all  $|\beta| \leq 0.3\sqrt{n}$ , with success probability  $1 - \delta$ . We determine the sample complexity through Monte Carlo resampling of the measurement results. Further details of the process reconstruction experiment are provided in Supplementary Material Sec. IV.

As shown in Fig. 2(c), entanglement in the form of two-mode squeezing significantly enhances the scaling

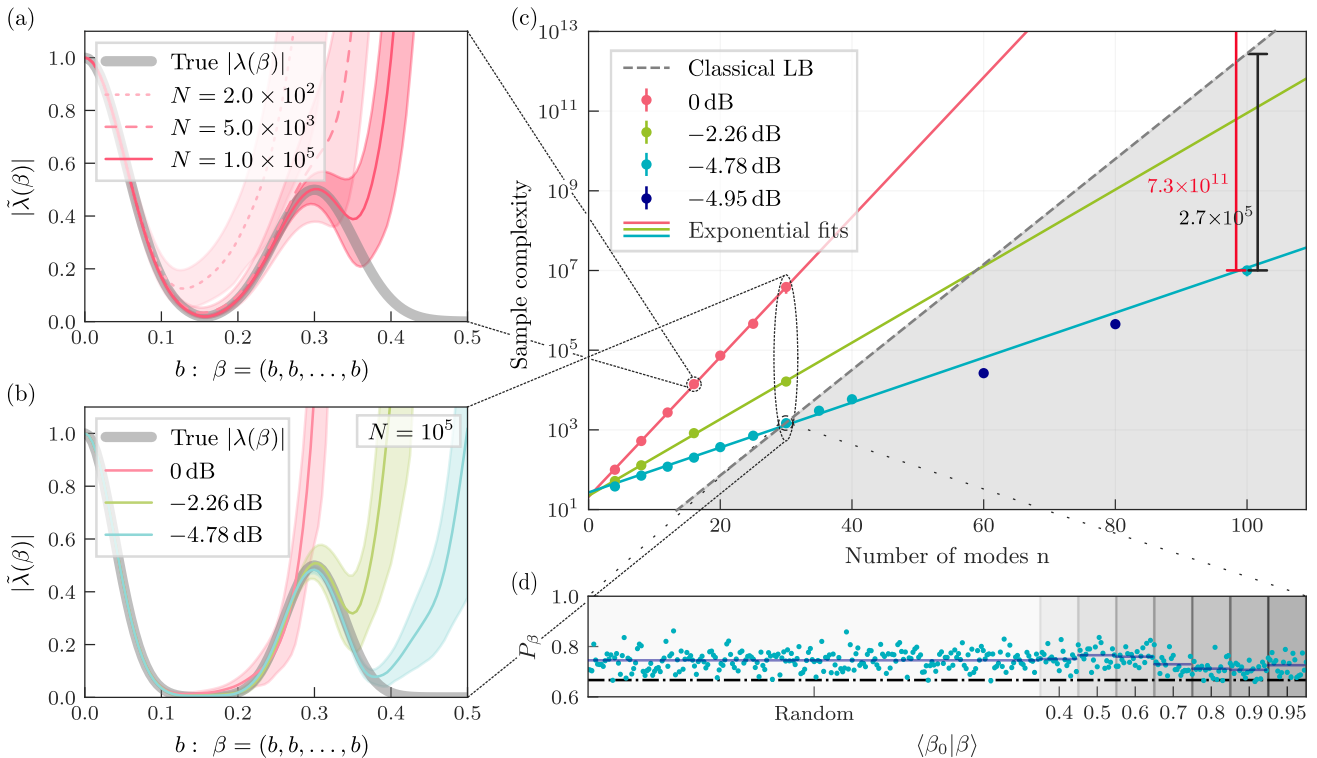


**Fig. 2. Reconstruction of a physical process.** (a) Experimentally reconstructed characteristic function  $\tilde{\lambda}(\beta)$  of an  $n = 16$ -mode three-peak process (defined in Supplementary Material, Definition S4) with fixed parameters using conventional measurement, compared with the true characteristic function  $\lambda(\beta)$ . The lines (shadings) show the average outcome ( $1\sigma$  standard deviation) of 100 runs of the reconstruction task using different numbers of samples. (b) Same as above, but using Bell measurement (with different amounts of squeezing). Here the number of modes is  $n = 30$  and we always use  $10^5$  samples for the same task. (c) Required number of samples to  $\epsilon$ -close reconstruct  $\lambda(\beta)$  of the three-peak process along the  $\beta_0$  direction with a success probability of  $1 - \delta = 2/3$ , versus the number of modes. The points are determined from experimental results, and the  $1\sigma$  standard deviation error bars are smaller than the data points. The solid lines are log-linear fits. The gray dashed line is the sample-complexity lower bound that applies to any entanglement-free strategy that can learn all processes in a large family which includes the process we studied. (d) Probability of achieving an  $\epsilon$ -close reconstruction of the  $-4.78$  dB, 30-mode characteristic function for various directions in the dual space. The shading highlights the proximity to the displacement direction  $\beta_0$ . Each probability is computed using  $N = 1472$  samples—same as required for an  $\epsilon$ -close reconstruction in (c). The dashed line indicates the target probability of  $1 - \delta$ .

of sample complexity, leading to substantial improvements as the number of modes increases. For  $n = 100$ , the sample complexity with the strongest squeezing ( $-4.78$  dB) remains about  $10^7$ . In contrast, from an exponential fit of low mode number data, we estimate that the entanglement-free scheme using vacuum states and heterodyne measurements would require a sample complexity as high as  $7.3 \times 10^{18}$  for the same task, or more than twenty million years for acquiring all the data if the samples are generated at the same rate (1 MHz per mode) as in our experiment. This represents an empirical improvement of 11.8 orders of magnitude.

Further, in Fig. 2(d) we confirm that the success probability of reconstructing  $\lambda(\beta)$  is the lowest along directions  $\beta$  that are close to  $\beta_0$ , i.e. in the direction of the distribution’s high-frequency peaks. Therefore, the sample complexity in Fig. 2(c) is a faithful estimation of the true complexity for learning this channel.

*Provable, scalable quantum advantage.*—Also shown in Fig. 2(c) is a lower bound on the sample complexity of entanglement-free learning schemes, derived in

Supplementary Material Sec. IIC. Compared to this bound, the entanglement-enhanced reconstruction of the 100-mode process uses more than five orders of magnitude fewer samples. However, the sample-complexity lower bound applies to entanglement-free schemes that can learn the characteristic function  $\lambda(\beta)$  accurately for any random displacement process in a large family, and for all values of  $\beta$  in a specified bounded range, while our experiment learns the characteristic function for processes chosen from a smaller family and for more restricted values of  $\beta$ . Therefore, the improved process reconstruction we achieved using entanglement does not demonstrate a provable quantum advantage.

To establish a provable quantum advantage, we consider the task of identifying specific features of an unknown process. Specifically, we design a hypothesis testing game (cf. Fig. 3(a)) where a dealer prepares several  $n$ -mode displacement processes  $\Lambda_k, k \in \{1, \dots, K\}$ . Each process may or may not exhibit a feature—specifically, two peaks at the locations  $\pm\gamma_k$  in its characteristic function. Depending on the ex-



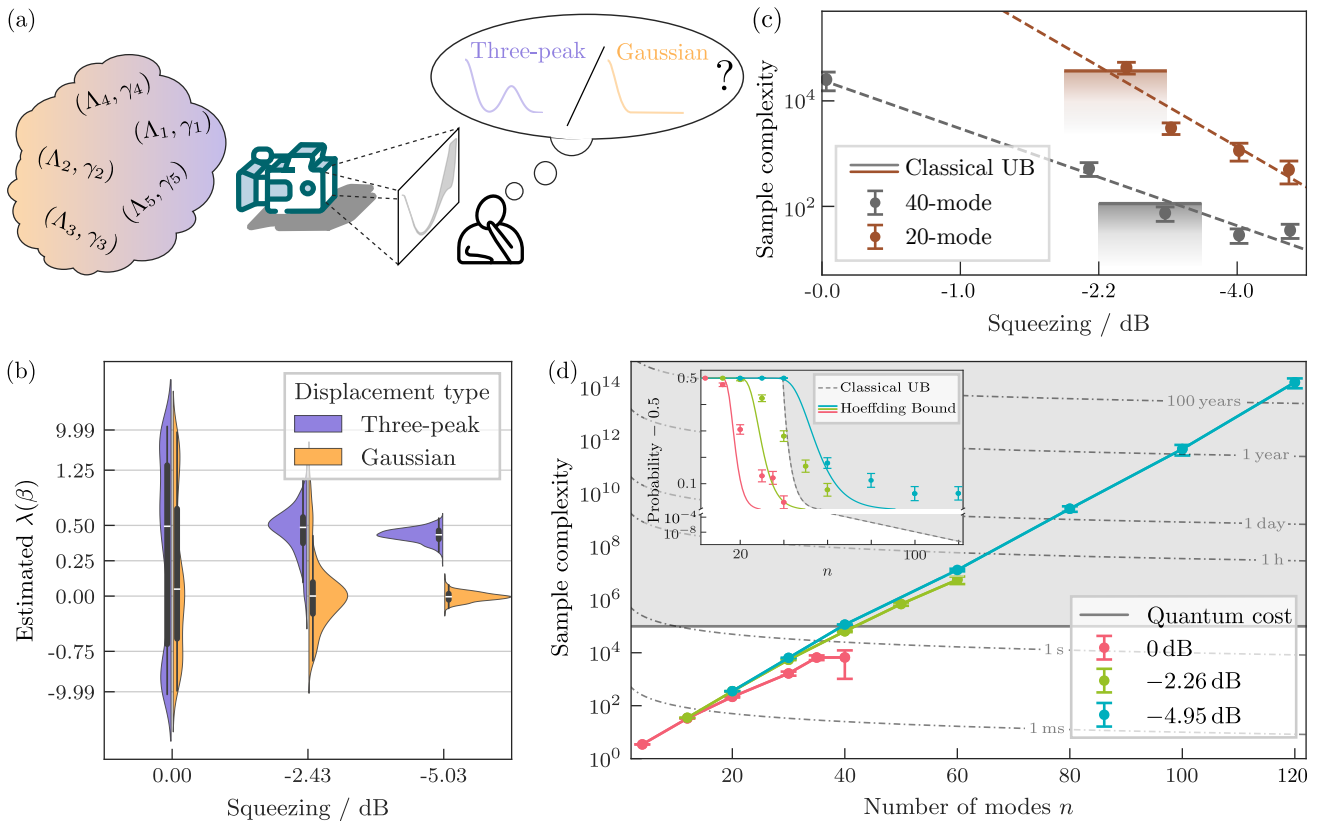


Fig. 3. **Hypothesis testing.** (a) The objective is to distinguish whether a displacement process belongs to the three-peak family with an unknown parameter or the Gaussian family. (b) An example of the separation of the estimator,  $\tilde{\lambda}(\beta = \gamma)$ , for two types of 40-mode displacement processes using different amounts of squeezing. In the noiseless case, the value is expected to be 0.5 (0) for three-peak (Gaussian) channel. (c) Sample complexity for achieving 2/3 success probability in a  $\kappa = 0.2$  hypothesis test, estimated with varying amounts of squeezing. The solid and dashed lines indicate the classical complexity bound for achieving the same success probability and the exponential fit, respectively. The shading indicates the region excluded by the classical complexity bound (see Supplementary Material Sec. VB for more details). (d) Inset: the measured probability of winning the  $\kappa = 0.2$  hypothesis testing game for different numbers of modes, using  $10^5$  samples and various amounts of squeezing. Solid lines represent a pessimistic estimation of success probability derived from the Hoeffding bound [8]. Main: Minimum sample complexity for any conventional strategy to achieve the same success probability as reported in the inset, calculated according to the classical complexity bound, and the corresponding sample collection time at a 1 MHz/mode rate. Error bars represent the  $1\sigma$  standard deviation from a 25-step sequential sampling. The shaded region indicates the existence of a quantum advantage.

istence or absence of these peaks, the processes are grouped into three-peak and Gaussian families, respectively (cf. Supplementary Material, Definitions 4 and 5). A challenger is allowed to implement each process  $N$  times. After all the measurements are finished, the dealer reveals  $\gamma_k$  and the challenger is asked to identify the family that the process belongs to. In the quantum strategy for the game, the challenger records the Bell measurement outcomes and computes the estimator  $\tilde{\lambda}(\beta)$  at  $\beta = \gamma_k$  once the value is announced. They then compare the value of  $\tilde{\lambda}(\beta)$  with a threshold  $\lambda_0$  to classify the process. If  $\tilde{\lambda}(\beta) > \lambda_0$  is observed, they will guess the process as three-peak type, and otherwise as Gaussian. The random nature of  $\gamma_k$  in the hypothesis testing game removes the excessive prior information. Consequently, an experimentally measured sample complexity surpassing the classical complexity bound can demonstrate a provable quantum advantage. On the other hand, the quantum strategy remains effective even if the challenger is unaware of  $\gamma_k$  during the measurement process, highlighting the

practicality of the approach.

We conducted a series of hypothesis testing games to conclusively observe the provable quantum advantage, with full details provided in Supplementary Material Sec. 4. In these games, the average distance of the peaks from the origin is proportional to  $\sqrt{\kappa n}$ , where the resolution constant  $\kappa = 0.2$  controls the hardness of the task. First, we fixed the number of samples at  $N = 10^5$  and classified a set of 40-mode processes using different levels of two-mode squeezing. The behavior of the estimators across these experiments is reported in Fig. 3(b). As the squeezing increases, the displacement signal becomes more pronounced against the noise, and the estimator distribution evolves from being almost random to strongly clustering around the true value. Next, we used the Monte Carlo method to determine the number of samples  $N$  required to achieve a success probability of 2/3 in 20-mode and 40-mode hypothesis testing games. As shown in Fig. 3(c), squeezing reduces the sample complexity in these tasks. Even at these modest mode numbers, a quantum advantage is

clearly observed.

Finally, we explore how the degree of quantum advantage scales with the number of modes of the displacement process. To do this, we measured the success probability of hypothesis testing with a fixed sample size of  $N = 10^5$ , then calculated the number of classical samples required to achieve the same success probability. A higher success probability corresponds to a larger equivalent classical sample complexity and demonstrates a stronger quantum advantage. As the number of modes increases, process classification becomes more challenging because the estimator diverges more rapidly for even smaller values of  $\beta$ . This behavior is illustrated in Fig. 3(d) inset, which shows that the success probability evolves through three phases for different squeezing levels: starting from  $\simeq 1$  in low mode number systems where the information from the displacement process dominates the noise, transitioning through a region of decline, and eventually converging to  $\simeq 0.5$  when noise prevails and the estimator “diverges” at  $\beta = \gamma$ , making the estimate no better than a coin toss. Importantly, increased squeezing shifts the transition region to higher mode numbers, allowing some data points to achieve success probability significantly above what is possible with classical strategies using the same number of samples. When the success probability significantly exceeds 0.5, we compute the equivalent classical sample complexity and compare with the  $10^5$  realized samples, which took  $n \times 0.1$  s to acquire. Our results, shown in Fig. 3(d), demonstrate the exponential scaling of classical sample complexity with the number of modes and emphasize how the quantum advantage increases as the number of modes grows. For the largest scale (120-mode) experiment, we measured a hypothesis testing success probability of  $0.563 \pm 0.025$ , exceeding the bound for conventional strategy ( $0.5 + 3.8 \times 10^{-11}$ ) with a confidence level of 99.3%. To learn one process and achieve the same success probability with a conventional approach,  $1.6 \times 10^{14}$  classical samples would be required. This translates into an expected measurement time of more than 600 years at a 1 MHz rate. Our result thus indicates a provable quantum advantage of 9.2 orders of magnitude.

*Outlook.*—In this work, we have demonstrated a sub-

stantial quantum advantage in learning using a scalable, albeit noisy and lossy, photonic platform based on EPR entangled states and CV Bell measurements. Despite system losses of approximately 20%, we achieved a quantum improvement exceeding 11 orders of magnitude compared to the classical approach of using coherent state probes and heterodyne detection. This translates into an expected reduction of measurement time from more than twenty million years to less than 15 minutes, assuming the modes are generated at 1 MHz frequency as in our experiment. Our method therefore enables the resolution of intricate features in highly complex systems, offering to potentially uncover hidden structures that would remain completely inaccessible with classical measurement techniques. Further, our research sheds light on a novel quantum learning framework, where the information to be learned is encoded into the temporal domain. This quantum learning framework invites further exploration both in theory and in experiments.

Looking ahead, our scalable photonic platform lays the foundation for tackling even more complex tasks. Future advancements in reducing losses, increasing squeezing levels, and integrating advanced photonic technologies could further enhance the capabilities of quantum learning protocols. The insights gained from our approach have the potential to drive significant progress in quantum-enhanced sensing, parameter estimation, and even quantum-enhanced machine learning algorithms, where photonic platforms are uniquely suited to tackle high-dimensional and continuous-variable problems. By leveraging quantum learning, these enhanced protocols could unlock unprecedented opportunities for scientific discovery and technological innovation.

While previous demonstrations of quantum advantage on noisy intermediate-scale photonic platforms have primarily focused on quantum computational tasks like Gaussian boson sampling, our work showcases a fundamentally different achievement: a significant quantum advantage in learning. This task extends beyond computation to encompass the understanding and characterization of physical systems, highlighting the versatility of photonic platforms and their critical role in advancing quantum technologies.

- 
- [1] L. Banchi, J. L. Pereira, S. T. Jose, and O. Simeone, *Statistical complexity of quantum learning*, *Advanced Quantum Technologies* **2024**, 2300311 (2023).
  - [2] A. Anshu and S. Arunachalam, *A survey on the complexity of learning quantum states*, *Nature Reviews Physics* **6**, 59 (2024).
  - [3] H. Y. Huang, R. Kueng, and J. Preskill, *Information-theoretic bounds on quantum advantage in machine learning*, *Physical Review Letters* **126**, 190505 (2021).
  - [4] D. Aharonov, J. Cotler, and X. L. Qi, *Quantum algorithmic measurement*, *Nature Communications* **13**, 887 (2022).
  - [5] S. Chen, S. Zhou, A. Seif, and L. Jiang, *Quantum advantages for Pauli channel estimation*, *Physical Review A* **105**, 032435 (2022).
  - [6] M. C. Caro, *Learning quantum processes and Hamiltonians via the Pauli transfer matrix*, *ACM Transactions on Quantum Computing* **5**, 14 (2022).
  - [7] Z. M. Rossi, J. Yu, I. L. Chuang, and S. Sugiura, *Quantum advantage for noisy channel discrimination*, *Physical Review A* **105**, 032401 (2022).
  - [8] C. Oh, S. Chen, Y. Wong, S. Zhou, H.-Y. Huang, J. A. Nielsen, Z.-H. Liu, J. S. Neergaard-Nielsen, U. L. Andersen, L. Jiang, and J. Preskill, *Entanglement-enabled advantage for learning a bosonic random displacement channel*, *Physical Review Letters* **133**, 230604 (2024).
  - [9] S. Chen, J. Cotler, H. Y. Huang, and J. Li, *Exponential separations between learning with and without quantum memory*, *Proceedings - Annual IEEE Symposium on Foundations of Computer Science, FOCS*

2022-February, 574 (2022).

- [10] A. Seif, S. Chen, S. Majumder, H. Liao, D. S. Wang, M. Malekakhlagh, A. Javadi-Abhari, L. Jiang, and Z. K. Mineev, *Entanglement-enhanced learning of quantum processes at scale* (2024), arXiv:2408.03376 [quant-ph].
- [11] H.-Y. Huang, M. Broughton, J. Cotler, S. Chen, J. Li, M. Mohseni, H. Neven, R. Babbush, R. Kueng, J. Preskill, and J. R. McClean, *Quantum advantage in learning from experiments*, *Science* **376**, 1182 (2022).
- [12] C. Weedbrook, S. Pirandola, R. García-Patrón, N. J. Cerf, T. C. Ralph, J. H. Shapiro, and S. Lloyd, *Gaussian quantum information*, *Reviews of Modern Physics* **84**, 621 (2012).
- [13] H.-S. Zhong, H. Wang, Y.-H. Deng, M.-C. Chen, L.-C. Peng, Y.-H. Luo, J. Qin, D. Wu, X. Ding, Y. Hu, P. Hu, X.-Y. Yang, W.-J. Zhang, H. Li, Y. Li, *et al.*, *Quantum computational advantage using photons*, *Science* **370**, 1460 (2020).
- [14] L. S. Madsen, F. Laudenbach, M. F. Askarani, F. Rortais, T. Vincent, J. F. Bulmer, F. M. Miatto, L. Neuhaus, L. G. Helt, M. J. Collins, A. E. Lita, T. Gerrits, S. W. Nam, V. D. Vaidya, M. Menotti, *et al.*, *Quantum computational advantage with a programmable photonic processor*, *Nature* **606**, 75 (2022).
- [15] M. Takeoka, S. Guha, and M. M. Wilde, *Fundamental rate-loss tradeoff for optical quantum key distribution*, *Nature Communications* **5**, 5235 (2014).
- [16] S. Pirandola, R. Laurenza, C. Ottaviani, and L. Banchi, *Fundamental limits of repeaterless quantum communications*, *Nature Communications* **8**, 15043 (2017).
- [17] S. Pirandola, U. L. Andersen, L. Banchi, M. Berta, D. Bunandar, R. Colbeck, D. Englund, T. Gehring, C. Lupo, C. Ottaviani, J. L. Pereira, M. Razavi, J. S. Shaari, M. Tomamichel, V. C. Usenko, *et al.*, *Advances in quantum cryptography*, *Advances in Optics and Photonics* **12**, 1012 (2020).
- [18] M. V. Larsen, X. Guo, C. R. Breum, J. S. Neergaard-Nielsen, and U. L. Andersen, *Deterministic multi-mode gates on a scalable photonic quantum computing platform*, *Nature Physics* **17**, 1018 (2021).
- [19] I. Tzitrin, T. Matsuura, R. N. Alexander, G. Dauphinais, J. E. Bourassa, K. K. Sabapathy, N. C. Menicucci, and I. Dhand, *Fault-tolerant quantum computation with static linear optics*, *PRX Quantum* **2**, 040353 (2021).
- [20] M. V. Larsen, C. Chamberland, K. Noh, J. S. Neergaard-Nielsen, and U. L. Andersen, *Fault-tolerant continuous-variable measurement-based quantum computation architecture*, *PRX Quantum* **2**, 030325 (2021).
- [21] M. Tse, H. Yu, N. Kijbunchoo, A. Fernandez-Galiana, P. Dupej, L. Barsotti, C. D. Blair, D. D. Brown, S. E. Dwyer, A. Effler, M. Evans, P. Fritschel, V. V. Frolov, A. C. Green, G. L. Mansell, *et al.*, *Quantum-enhanced advanced LIGO detectors in the era of gravitational-wave astronomy*, *Physical Review Letters* **123**, 231107 (2019).
- [22] X. Guo, C. R. Breum, J. Borregaard, S. Izumi, M. V. Larsen, T. Gehring, M. Christandl, J. S. Neergaard-Nielsen, and U. L. Andersen, *Distributed quantum sensing in a continuous-variable entangled network*, *Nature Physics* **16**, 281 (2020).
- [23] J. A. Nielsen, J. S. Neergaard-Nielsen, T. Gehring, and U. L. Andersen, *Deterministic quantum phase estimation beyond  $N00N$  states*, *Physical Review Letters* **130**, 123603 (2023).
- [24] C. Oh, M. Liu, Y. Alexeev, B. Fefferman, and L. Jiang, *Classical algorithm for simulating experimental Gaussian boson sampling*, *Nature Physics* **20**, 1461 (2024).
- [25] J. J. Wallman and J. Emerson, *Noise tailoring for scalable quantum computation via randomized compiling*, *Physical Review A* **94**, 052325 (2016).
- [26] D. Ganapathy, W. Jia, M. Nakano, V. Xu, N. Aritomi, T. Cullen, N. Kijbunchoo, S. E. Dwyer, A. Mullavey, L. McCuller, R. Abbott, I. Abouelfettouh, R. X. Adhikari, A. Ananyeva, S. Appert, *et al.* (LIGO O4 Detector Collaboration), *Broadband quantum enhancement of the LIGO detectors with frequency-dependent squeezing*, *Phys. Rev. X* **13**, 041021 (2023).
- [27] C. H. Valahu, T. Navickas, M. J. Biercuk, and T. R. Tan, *Benchmarking bosonic modes for quantum information with randomized displacements* (2024), arXiv:2405.15237 [quant-ph].
- [28] J.-X. Cheng and X. S. Xie, *Vibrational spectroscopic imaging of living systems: An emerging platform for biology and medicine*, *Science* **350**, aaa8870 (2015).
- [29] R. B. de Andrade, H. Kerdoncuff, K. Berg-Sørensen, T. Gehring, M. Lassen, and U. L. Andersen, *Quantum-enhanced continuous-wave stimulated raman scattering spectroscopy*, *Optica* **7**, 470 (2020).
- [30] K. M. Backes, D. A. Palken, S. A. Kenany, B. M. Brubaker, S. B. Cahn, A. Droster, G. C. Hilton, S. Ghosh, H. Jackson, S. K. Lamoreaux, A. F. Leder, K. W. Lehnert, S. M. Lewis, M. Malnou, R. H. Maruyama, *et al.*, *A quantum enhanced search for dark matter axions*, *Nature* **590**, 238 (2021).
- [31] A. J. Brady, C. Gao, R. Harnik, Z. Liu, Z. Zhang, and Q. Zhuang, *Entangled sensor-networks for dark-matter searches*, *PRX Quantum* **3**, 030333 (2022).
- [32] S. Barzanjeh, A. Xuereb, S. Gröblacher, M. Paternostro, C. A. Regal, and E. M. Weig, *Optomechanics for quantum technologies*, *Nature Physics* **18**, 15 (2022).

**Acknowledgements.**—We thank Huy Quang Nguyen and Benjamin Lundgren Larsen for the help with the experiment. We gratefully acknowledge support from the Danish National Research Foundation, Center for Macroscopic Quantum States (bigQ, DNR0142), EU project CLUSTEC (grant agreement no. 101080173), EU ERC project ClusterQ (grant agreement no. 101055224), NNF project CBQS, Innovation Fund Denmark (PhotoQ project, grant no. 1063-00046A), and the MSCA European Postdoctoral Fellowships (GTGBS, project no. 101106833). J.P. acknowledges support from the U.S. Department of Energy Office of Science, Office of Advanced Scientific Computing Research (DE-NA0003525, DE-SC0020290), the U.S. Department of Energy, Office of Science, National Quantum Information Science Research Centers, Quantum Systems Accelerator, and the National Science Foundation (PHY-1733907). The Institute for Quantum Information and Matter is an NSF Physics Frontiers Center. L.J. acknowledges support from the ARO(W911NF-23-1-0077), ARO MURI (W911NF-21-1-0325), AFOSR MURI (FA9550-19-1-0399, FA9550-21-1-0209, FA9550-23-1-0338), DARPA (HR0011-24-9-0359, HR0011-24-9-0361), NSF (OMA-1936118, ERC-1941583, OMA-2137642, OSI-2326767, CCF-2312755), NTT Research, and the Packard Foundation (2020-71479). S.Z. acknowledges funding provided by Perimeter Institute for Theoretical Physics, a research institute supported in part by the Govern-

ment of Canada through the Department of Innovation, Science and Economic Development Canada and by the Province of Ontario through the Ministry of Colleges and Universities. C.O. acknowledges support from Quantum Technology R&D Leading Program

(Quantum Computing) (RS-2024-00431768) through the National Research Foundation of Korea (NRF) funded by the Korean government [Ministry of Science and ICT (MSIT)].